

Perpendicular subcritical shock structure in a collisional plasma experiment

D. R. Russell,^{1,*} G. C. Burdiak,² J. J. Carroll-Nellenback,³ J. W. D. Halliday,¹ J. D. Hare,⁴
 S. Merlini,¹ L. G. Suttle,¹ V. Valenzuela-Villaseca,¹ S. J. Eardley,¹ J. A. Fullalove,¹ G. C.
 Rowland,¹ R. A. Smith,¹ A. Frank,³ P. Hartigan,⁵ A. L. Velikovich,⁶ and S. V. Lebedev¹

¹*Blackett Laboratory, Imperial College London, London SW7 2AZ, United Kingdom*

²*First Light Fusion Ltd, Yarnton, Kidlington OX5 1QU, United Kingdom*

³*Department of Physics and Astronomy, University of Rochester, Rochester, NY 14627, USA*

⁴*Plasma Science and Fusion Center, Massachusetts Institute of Technology, Cambridge MA 02139, USA*

⁵*Department of Physics and Astronomy, Rice University, Houston, TX 77005-1892, USA*

⁶*Plasma Physics Division, Naval Research Laboratory, Washington, DC 20375, USA*

(Dated: January 25, 2022)

We present a study of perpendicular subcritical shocks in a collisional laboratory plasma. Shocks are produced by placing obstacles into the super-magnetosonic outflow from an inverse wire array z-pinch. We demonstrate the existence of subcritical shocks in this regime and find that secondary shocks form in the downstream. Detailed measurements of the subcritical shock structure confirm the absence of a hydrodynamic jump. We calculate the classical (Spitzer) resistive diffusion length and show that it is approximately equal to the shock width. We measure little heating across the shock ($< 10\%$ of the ion kinetic energy) which is consistent with an absence of viscous dissipation.

Shock waves are ubiquitous in astrophysical [1], space [2] and laboratory plasmas and often include an embedded, dynamically significant magnetic field. The theoretical understanding of magneto-hydrodynamic (MHD) shock waves was first established in the 1950s [3–6]. In particular, it was discovered that resistive Ohmic heating, a dissipation mechanism specific to MHD, can shape shock structures. Since resistivity does not directly dissipate the plasma kinetic energy, there is a critical value of the upstream magnetosonic Mach number, M_C , indicating the maximum strength of MHD shocks shaped by Ohmic heating alone. This is defined by setting the downstream sonic Mach number $M_{S,d} = 1$ [7, 8]. The downstream flow is supersonic for subcritical shocks, and hydrodynamic parameters are continuous across the shock.

Since then, studies of subcritical shocks have focused on the collisionless regime [9, 10], motivated by the ubiquity of collisionless shocks in space and astrophysical plasmas. In these cases, the physical processes which generate entropy at the shock are more complicated than the collisional transport models [11, 12]. This leads to difficulty in defining the critical Mach number (due to the lack of downstream thermodynamic equilibrium) and determining the plasma resistivity. Recent progress in magneto-inertial fusion [13–16], has stimulated renewed interest in MHD shocks propagating through dense, collision-dominated plasmas. In particular, recent experiments studying the implosion of magnetised inertial confinement fusion capsules have shown an increased yield and anisotropic shock structure [17, 18]. The structures of MHD shocks in this regime have been investigated theoretically [19, 20] but never measured experimentally.

This letter reports the first experimental study of subcritical shock structure in a highly collisional plasma (m.f.p. \ll shock width). A supersonic ($M_S \sim 2.5$),

super-Alfvénic ($M_A \sim 3$) plasma flow was produced by the current driven ablation of an inverse wire array z-pinch [21], and shocks were studied by placing stationary obstacles into this flow [22]. The orientation of the obstacles produced perpendicular shocks, in which the advected magnetic field was perpendicular to the shock normal. Subcritical shocks were observed in which the downstream flow is shown to be supersonic. These measurements of a subcritical shock in a collisional plasma are the first of their kind and confirm the absence of a hydrodynamic jump as predicted by theory (e.g. [8, 20]). Furthermore, detailed laser probing measurements allow calculation of the resistive diffusion length, L_η (using classical Spitzer resistivity) which we show to be approximately equal to the shock width. The shock structure can therefore be described by classical resistive MHD, without the inclusion of anomalous resistivity. We observed little plasma heating at the shock ($< 10\%$ of the ion kinetic energy) consistent with a balance between adiabatic and Ohmic heating and radiative cooling.

The experimental setup is shown in Fig. 1. The inverse wire array z-pinch was driven by the MAGPIE pulsed power generator (1.4 MA peak current, 240 ns rise time) [23]. A cylindrical arrangement (21 mm high and 20 mm in diameter) of 21 aluminium wires (each with a 40 μm diameter) surrounded a central cathode. This experimental geometry provided a $\mathbf{J} \times \mathbf{B}$ force which acted radially outwards, accelerating the plasma ablated by the wires for the duration of the drive current [24]. Since some of the drive current passed through the ablated plasma surrounding each wire, a fraction of the magnetic field was advected by the flow [25]. The 11 wires closest to the obstacles had an angular separation of 11.25° while the remaining wires had an angular separation of 22.5° , see Fig. 1 (b). The smaller wire separation reduced azimuthal density variation by reducing the divergence of

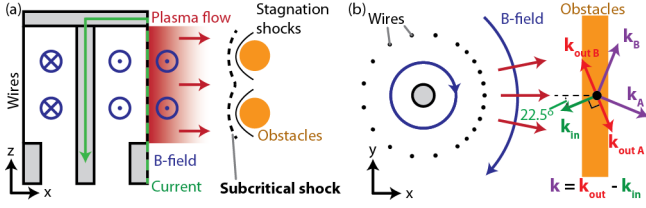


FIG. 1. Cross-sectional diagram of the wire array and obstacles. (a) Side-on view. Cylindrical obstacles extend into the page and shocks are indicated where they form in the experiment. (b) End-on view showing the azimuthal configuration of wires in the array and the vector diagram for the Thomson scattering diagnostic.

the flow and allowing outflows from adjacent wires to merge [22].

Two 4 mm diameter cylindrical brass obstacles were placed 10 mm from the ablating wires and were oriented with their axes parallel to the advected magnetic field (Fig. 1). The obstacles had a centre-to-centre separation of 9 mm in the vertical, z , direction and were 40 mm in length. The obstacles produced shocks in the plasma flow which were extended in the y direction and approximately stationary in the laboratory frame for ~ 200 ns (many hydrodynamic crossing times).

Electron density was measured using a Mach-Zehnder laser interferometer (532 nm, 0.4 ns FWHM). The analysis method is described in Refs. [26, 27]. An electron density map in the x - z plane is presented in Fig. 2 (a). The line averaged electron density was calculated by $n_e \approx \int n_e dy / L$ where the choice $L = 40$ mm is consistent with interferometry measurements in the x - y plane.

The observed shock structure comprises two distinct types of shock. A subcritical shock spans the region upstream of both obstacles. This shock is smooth and continuous between the obstacles. Fast-frame optical self-emission imaging has shown that this shock forms as a single shock ~ 300 ns after current start [22, 24]. In addition to the subcritical shock, two secondary shocks, referred to here as stagnation shocks, form closer to the obstacles, downstream of the subcritical shock. These do not expand upstream to reach the position of the subcritical shock. The stagnation shocks cause a more abrupt density increase than the subcritical shock.

The magnetic field distribution in the x - z plane was measured using a Faraday rotation imaging diagnostic in combination with inline interferometry (1053 nm, 1 ns FWHM). The diagnostic is described in Ref. [26] and the analysis in Ref. [28]. The measurement is sensitive to the line averaged, electron density weighted B_y component of the magnetic field. This is the dominant component in the shock region, however, we expect some curvature of the magnetic field due to the cylindrical structure of the wire array, so Faraday rotation imaging provides a lower bound for B_y at $y = 0$ mm. Fig. 2 (b) shows

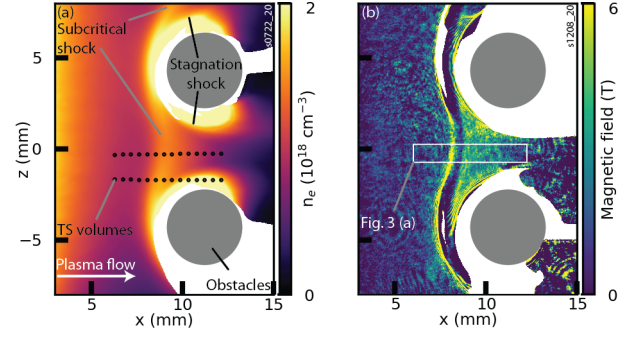


FIG. 2. Electron density and magnetic field measurements. (a) Electron density recorded 426 ns after current start. The edge of the wire array is at $x = 0$ mm. (b) Magnetic field 397 ns after current start. The region sampled by the lineout in Fig. 3 is shown.

the measured magnetic field. In the region between the obstacles, the magnetic field increases from 1.5 – 2 T upstream of the subcritical shock to 3 – 4 T in the downstream, showing that magnetic field is compressed across the shock. Redistribution of the laser intensity caused by refraction at density gradients (shadowgraphy) leads to an intensity modulation at the subcritical shock ramp so magnetic field cannot be inferred inside the shock.

Optical Thomson Scattering (TS) of the ion acoustic feature provided localised measurements of plasma velocity and temperatures [26, 29]. A focused laser beam (532 nm, 8 ns FWHM, 200 μ m beam waist) passed between the obstacles at 22.5° to the x -axis in the x - y plane (\mathbf{k}_{in} in Fig. 1 (b)). The scattered light was imaged onto two separate arrays of 14 optical fibres at $\pm 90^\circ$ to the laser beam ($\mathbf{k}_{out A}$ and $\mathbf{k}_{out B}$), which recorded the scattered spectra from the same 14 localised plasma volumes (shown in Fig. 2 (a)). The Doppler shifted spectra are sensitive to the velocity components along \mathbf{k}_A and \mathbf{k}_B . Temperatures and velocities were inferred by fitting theoretical spectra to the experimental data [30, 31].

The flow velocity directly upstream of the subcritical shock was 45 km s^{-1} and the temperature was $T_e = T_i = 11 \pm 3 \text{ eV}$ (self consistent values of T_e and \bar{Z} were inferred from the experimentally measured $\bar{Z}T_e$ using an nLTE atomic model [32]). The fact that we measure $T_e = T_i$ is unsurprising since the thermal equilibration time $\tau_{i/e} \sim 5$ ns.

Combined analysis of interferometry, Faraday rotation and TS data allow characteristic dimensionless parameters of the upstream plasma to be calculated, see Table I. The thermal and magnetic pressures differ by less than a factor 2, while the ram pressure is substantially larger. The Mach numbers all exceed unity so the flow will form a shock when colliding with stationary obstacles. The critical Mach number (which depends on β_{th} and the shock angle [33]) for these upstream parameters is $M_C \sim 1.4$ (assuming $\gamma = 5/3$). However, we note that only a small

Dimensionless parameter		Value
Thermal beta	β_{th}	1.7
Dynamic beta	β_{ram}	18
Sonic Mach number	M_S	2.5
Alfvénic Mach number	M_A	3
Magnetosonic Mach number	M_{MS}	1.9
Reynolds number	Re	4×10^4
Magnetic Reynolds number	Re_M	$10 \rightarrow 1$

TABLE I. Characteristic plasma parameters upstream of the subcritical shock ~ 400 ns after current start. $\beta_{th} = P_{th}/P_{mag}$ and $\beta_{ram} = P_{ram}/P_{mag}$. To evaluate the magnetic Reynolds number, a scale length of 10 mm, the distance between the wire array and the obstacles, gives $Re_M \sim 10$ while a distance of ~ 0.8 mm, the subcritical shock width, gives $Re_M \sim 1$.

increase in the magnetic field, to 2.2 T, would be required for the flow to be subcritical with respect to a stationary shock (giving $M_{MS} = 1.7$ and $\beta_{th} = 1$). Since the magnetic field inferred from the Faraday rotation data gives a lower bound for $B_y(y = 0 \text{ mm})$, we conclude that a subcritical shock may form. The large Reynolds number means viscous dissipation will occur on scales much smaller than the system size. However, the modest value of Re_M shows that while magnetic field is expected to be advected in the upstream, magnetic diffusion will become important on the spatial scale of the shocks.

Fig. 3 (a) and (b) show the velocity and temperature measurements from TS in the $z = 0$ mm plane alongside lineouts of electron density and magnetic field (the locations of the TS scattering volumes are shown in Fig. 2 (a)). The electron density increases across the subcritical shock before decreasing as the plasma expands into the vacuum behind the shock. The velocity, which was measured locally, is consistent with 1D conservation of mass, suggesting that line integration does not affect the interferometry result. The ion and electron temperatures are equal across the shock and change by less than 10 eV ($T = T_e = T_i$ is presented in Fig. 3 (b)).

We characterise the subcritical shock in terms of the density compression ratio and the shock width. The compression ratio, R , is estimated from electron density measurements. The compression ratio is estimated by comparing the downstream density in experiments with obstacles to the density at the same x location in an experiment without obstacles (null shot), which yields $R = 2.7 \pm 0.5$. This is consistent with the MHD shock jump conditions for all reasonable values of γ .

The measured shock width, defined as the distance between 10% and 90% of the density jump, was 0.87 ± 0.08 mm. The width of a shock is determined by the dissipative and/or dispersive processes which increase entropy and transport energy at the shock front [34]. Table II shows a comparison of the shock width with characteristic length scales for viscous dissipation ($\lambda_{i,i}$), Ohmic dissipation (L_η), electron heat conduction (L_χ), and the

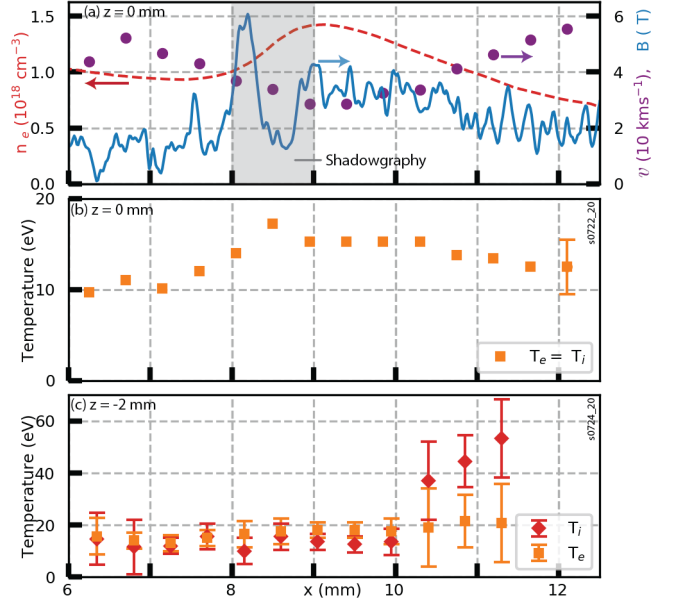


FIG. 3. Thomson scattering data and plasma parameter profiles. (a) Flow velocity at 416 ns with electron density and magnetic field lineouts at $z = 0$ mm. The region in which the magnetic field measurement was affected by shadowgraphy is shaded. (b) Temperature at $z = 0$ mm. A characteristic error bar which includes modeling uncertainty is shown for the final data point. (c) Ion and electron temperatures at $z = -2$ mm.

formation of a cross shock potential due to two-fluid effects (d_i).

The ion-ion mean free path is ~ 4 orders of magnitude smaller than the shock width. This indicates that viscous dissipation does not shape the shock structure and that the shock is subcritical. Resistive diffusion, heat conduction and two-fluid effects may all contribute to the shaping of a subcritical shock and their characteristic scale lengths are all comparable to the shock width. The largest dissipative scale, and the scale closest to the shock width is L_η . This suggests that Ohmic dissipation plays the most significant role in shock shaping. Since L_η is approximately equal to the shock width, the shock structure can be described by classical (Spitzer) resistive MHD only, without including anomalous resistivity. The contribution of electron heat conduction to shock shaping will be less than that of Ohmic dissipation since $L_\eta \sim 5 \times L_\chi$ in the upstream and $L_\eta > L_\chi$ across the entire subcritical shock. Two-fluid effects may also contribute to shock structure since d_i is also approximately equal to the shock width. The formation of a cross shock potential due to two-fluid separation is a dispersive effect and does not dissipate kinetic energy. Rather, it excites whistler waves which carry energy away from the shock front. Since the dispersive scale, d_i , is approximately equal to the largest dissipative scale, L_η , this energy will be quickly dissipated and will not result in shock oscillations typical of collisionless systems. We note that while

Parameter		Value (mm)
Shock width		0.87 ± 0.08
Ion-ion m.f.p	$\lambda_{i,i}$	8×10^{-5}
Resistive diffusion length	L_η	0.75
Electron thermal diffusion length	L_χ	0.16
Ion inertial length	d_i	0.69

TABLE II. Comparison of the measured shock width with characteristic dissipative and dispersive scale lengths.

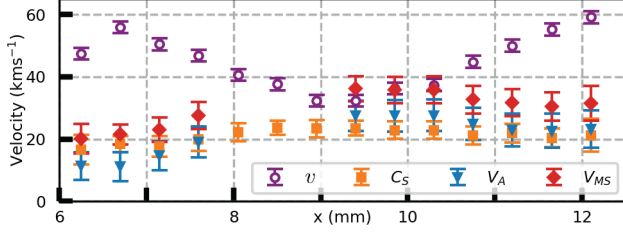


FIG. 4. Flow velocity compared with the sound speed, C_s , Alfvén speed, V_A , and fast-magnetosonic speed, V_{MS} , across the subcritical shock. Values which depend on B are excluded for $x = 8 - 9$ mm where Faraday rotation measurements are affected by shadowgraphy.

heat conduction and two-fluid effects may well contribute to shock structure, resistive diffusion alone is sufficient to explain the observed shock width.

The sound speed, Alfvén speed and fast-magnetosonic speed are compared with the flow velocity in Fig. 4. The flow becomes sub-magnetosonic across the shock but remains supersonic, a key signature of a subcritical shock. As the flow passes the obstacles, it expands into the vacuum and becomes super-magnetosonic again.

Since viscous dissipation does not shape the subcritical shock, the main heating mechanisms will be adiabatic and Ohmic. We estimate the heating due to adiabatic compression by calculating $T_2 = T_1 \times R^{\gamma-1} = 23 \pm 3$ eV for $\gamma = 5/3$. Ohmic heating will also increase the temperature and the heating power per unit volume can be estimated by

$$P = \eta J^2 = \eta \left(\frac{c}{4\pi} \right)^2 |\nabla \times B|^2, \quad (1)$$

where η is the Spitzer resistivity and $\nabla \times B \approx \Delta B_y / \Delta x \approx 2$ T/1 mm. This yields an increase in electron temperature of ~ 20 eV at the subcritical shock (assuming a velocity of 40 km s $^{-1}$). However, we note that the radiative cooling time (~ 10 ns [35]) is less than the time the plasma takes to cross the shock (~ 25 ns) so radiative cooling will reduce the observed temperature change. The estimated heating rate due to compression and Ohmic heating is ~ 40 eV/25 ns = 1.6 eV ns $^{-1}$. Balancing this against the radiative cooling rates presented in Ref. [35] requires an electron temperature of ~ 15 eV, in good agreement with the experimental results.

Behind the subcritical shock, the stagnation shock wings are stationary and remain downstream of the subcritical shock for the duration of the experiment. This suggests that the relevant Mach number for the stagnation shocks is the sonic Mach number, since this remains greater than unity across the subcritical shock. In this case, the stagnation shocks should be hydrodynamic jumps, formed by viscous dissipation on a spatial scale comparable to $\lambda_{i,i}$. This is below the resolution of the interferometry diagnostic (~ 0.5 mm), but TS measurements provide strong evidence for this interpretation. Fig. 3 (c) shows TS temperature measurements collected in the x - y plane at $z = -2$ mm which cross a stagnation shock (see locations of scattering volumes in Fig. 2 (a)). The measurements are consistent with those at $z = 0$ mm in the upstream and subcritical shock, but show substantial ion heating to $40 - 70$ eV at the stagnation shock. The flow velocity decreases to ~ 10 km s $^{-1}$ in this region and becomes subsonic. Both the ion heating and the subsonic downstream flow indicate that, in contrast to the subcritical shock, viscous dissipation of kinetic energy into ion thermal energy shapes the stagnation shocks.

To further investigate the role of resistive diffusion in shaping the subcritical shock, 2D simulations were carried out using AstroBEAR [36, 37], an adaptive mesh refinement (AMR) MHD code including resistivity and radiative loss. The two obstacles were simulated as 4 mm diameter perfectly conducting internal reflection boundaries with a centre-to-centre separation of 9 mm and were 20 mm from the left hand wall. A constant plasma flow was injected from the this wall and the three remaining boundaries were zero gradient boundaries. Two levels of AMR gave an effective resolution of 0.125 mm. The properties of the plasma wind, including resistivity, were varied to study the physics of the observed shocks. Radiative cooling was implemented by using the lookup table for aluminium presented in Ref. [35]. We study the shocks which formed 500 ns after the initial wind injection. By this time the shocks were well established and slow moving in the obstacle frame.

Fig. 5 shows results from two different simulations. In (a, c) the resistive diffusion length was 0.5 mm upstream of the shock. The upstream plasma parameters were $B = 4.5$ T, $n_e = 0.6 \times 10^{18}$ cm $^{-3}$, $v = 70$ km s $^{-1}$, $T = 7$ eV and $M_{MS} = 1.5$ (comparable to the experimental value). The simulation reproduced the morphology of the experiment, with a smooth and continuous subcritical shock forming upstream of both obstacles. The shock width was 2.2 mm. This suggests that, as in the experiments, viscous dissipation does not shape the shock. In contrast, (b, d) show a simulation with the same initial conditions but $\eta = 0$. In this case $\lambda_{i,i}$ exceeds L_η (which is zero) so the shock width is set by viscous dissipation and is limited by the simulation resolution. This shows that resistive diffusion does indeed set the shock width in (a, c), with a shock width comparable to the classical

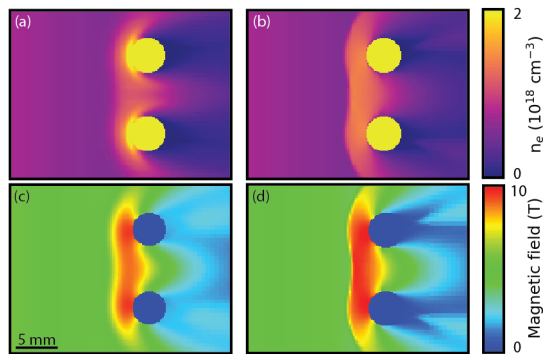


FIG. 5. Simulation results at 500 ns showing electron density and magnetic field with (a, c) $L_\eta = 0.5$ mm and (b, d) $L_\eta = 0$ mm.

resistive diffusion length.

In summary, we have presented an investigation of perpendicular subcritical shocks in a collisional plasma with $M_{MS} \sim 1.9$ and $\lambda_{i,i} \ll L_\eta$. We demonstrate that the shock is subcritical by showing that $M_S > 1$ across the shock. We confirm the theoretically predicted absence of a hydrodynamic jump, and show that the shock width is approximately equal to the classical (Spitzer) resistive diffusion length. We observe little heating at the subcritical shock, which is consistent with an absence of viscous dissipation. In contrast, downstream stagnation shocks cause substantial ion heating and produce a subsonic downstream flow. We interpret these shocks to be hydrodynamic in nature. Two-dimensional resistive MHD simulations reproduce the experimentally observed morphology of the subcritical shocks and demonstrate that Ohmic dissipation sets the shock width, which is comparable to the classical resistive diffusion length.

This work was supported by First Light Fusion Ltd. and by the US Department of Energy (DoE) including awards no. DE-NA0003764 and DE-SC0020434.

* daniel.russell13@imperial.ac.uk

- [1] R. A. Treumann, Fundamentals of collisionless shocks for astrophysical application, 1. Non-relativistic shocks, *Astronomy and Astrophysics Review* **17**, 409 (2009).
- [2] D. Burgess and M. Scholer, *Collisionless Shocks in Space Plasmas: Structure and Accelerated Particles* (Cambridge University Press, Cambridge, 2015).
- [3] F. D. Hoffmann and E. Teller, Magneto-Hydrodynamic Shocks, *Physical Review* **80**, 692 (1950).
- [4] P. Germain, Shock Waves and Shock-Wave Structure in Magneto-Fluid Dynamics, *Reviews of Modern Physics* **32**, 951 (1960).
- [5] R. V. Polovin, Shock Waves in Magnetohydrodynamics, *Soviet Physics Uspekhi* **3**, 677 (1961).
- [6] J. E. Anderson, *Magnetohydrodynamic shock waves* (MIT Press, Cambridge, MA, 1963).
- [7] W. Marshall, The structure of magneto-hydrodynamic shock waves, *Proceedings of the Royal Society of London. Series A. Mathematical and Physical Sciences* **233**, 367 (1955).
- [8] F. V. Coroniti, Dissipation discontinuities in hydromagnetic shock waves, *Journal of Plasma Physics* **4**, 265 (1970).
- [9] M. M. Mellott and E. W. Greenstadt, The structure of oblique subcritical bow shocks: ISEE 1 and 2 observations, *Journal of Geophysical Research: Space Physics* **89**, 2151 (1984).
- [10] D. B. Schaeffer, E. T. Everson, A. S. Bondarenko, S. E. Clark, C. G. Constantin, D. Winske, W. Gekelman, and C. Niemann, Experimental study of subcritical laboratory magnetized collisionless shocks using a laser-driven magnetic piston, *Physics of Plasmas* **22**, 113101 (2015).
- [11] S. I. Braginskii, Transport processes in a plasma, *Reviews of Plasma Physics* **1**, 205 (1965).
- [12] E. M. Epperlein and M. G. Haines, Plasma transport coefficients in a magnetic field by direct numerical solution of the Fokker-Planck equation, *The Physics of Fluids* **29**, 1029 (1998).
- [13] G. A. Wurden, S. C. Hsu, T. P. Intrator, T. C. Grabowski, J. H. Degnan, M. Domonkos, P. J. Turchi, E. M. Campbell, D. B. Sinars, M. C. Herrmann, R. Betti, B. S. Bauer, I. R. Lindemuth, R. E. Siemon, R. L. Miller, M. Laberge, and M. Delage, Magneto-Inertial Fusion, *Journal of Fusion Energy* **35**, 69 (2015).
- [14] S. A. Slutz, M. C. Herrmann, R. A. Vesey, A. B. Sefkow, D. B. Sinars, D. C. Rovang, K. J. Peterson, and M. E. Cuneo, Pulsed-power-driven cylindrical liner implosions of laser preheated fuel magnetized with an axial field, *Physics of Plasmas* **17**, 056303 (2010).
- [15] M. R. Gomez, S. A. Slutz, C. A. Jennings, D. J. Ampleford, M. R. Weis, C. E. Myers, D. A. Yager-Elorriaga, K. D. Hahn, S. B. Hansen, E. C. Harding, A. J. Harvey-Thompson, D. C. Lamppa, M. Mangan, P. F. Knapp, T. J. Awe, G. A. Chandler, G. W. Cooper, J. R. Fein, M. Geissel, M. E. Glinsky, W. E. Lewis, C. L. Ruiz, D. E. Ruiz, M. E. Savage, P. F. Schmit, I. C. Smith, J. D. Styron, J. L. Porter, B. Jones, T. R. Mattsson, K. J. Peterson, G. A. Rochau, and D. B. Sinars, Performance Scaling in Magnetized Liner Inertial Fusion Experiments, *Physical Review Letters* **125**, 155002 (2020).
- [16] L. J. Perkins, D. D.-M. Ho, B. G. Logan, G. B. Zimmerman, M. A. Rhodes, D. J. Strozzi, D. T. Blackfield, and S. A. Hawkins, The potential of imposed magnetic fields for enhancing ignition probability and fusion energy yield in indirect-drive inertial confinement fusion, *Physics of Plasmas* **24**, 062708 (2017).
- [17] J. D. Moody, B. B. Pollock, H. Sio, D. J. Strozzi, D. D. M. Ho, C. A. Walsh, E. Kemp, S. O. Kucheyev, B. Kozioziemski, E. G. Carroll, J. Fry, V. Tang, J. Javedani, A. Johnson, W. Stygar, C. Provencher, S. D. Bhandarkar, J. Sater, L. Hagler, G. B. Logan, J. D. Bude, M. C. Herrmann, K. Skulina, S. E. Winters, E. P. Hartouni, L. Divol, J. P. Chittenden, S. O'Neill, B. D. Appelbe, A. Boxall, A. J. Crilly, J. R. Davies, J. L. Peebles, A. Bose, and S. Fujioka, Progress on the magnetized ignition experimental platform for the National Ignition Facility, *Bulletin of the American Physical Society* (2021).
- [18] D. Ho, G. Zimmerman, A. Velikovich, R. Kulsrud, J. Moody, J. Harte, and A. Kritcher, Magnetized ICF: role of e-thermal conductivity on imploding shock and high-yield capsule designs, *Bulletin of the American*

- Physical Society (2021).
- [19] C. F. Kennel, Shock structure in classical magnetohydrodynamics, *Journal of Geophysical Research: Space Physics* **93**, 8545 (1988).
 - [20] M. A. Liberman and A. L. Velikovich, *Physics of Shock Waves in Gases and Plasmas* (Springer-Verlag, Berlin, 1986).
 - [21] A. J. Harvey-Thompson, S. V. Lebedev, S. N. Bland, J. P. Chittenden, G. N. Hall, A. Marocchino, F. Suzuki-Vidal, S. C. Bott, J. B. Palmer, and C. Ning, Quantitative analysis of plasma ablation using inverse wire array Z pinches, *Physics of Plasmas* **16**, 1 (2009).
 - [22] G. C. Burdiak, S. V. Lebedev, S. N. Bland, T. Clayson, J. Hare, L. Suttle, F. Suzuki-Vidal, D. C. Garcia, J. P. Chittenden, S. Bott-Suzuki, A. Ciardi, A. Frank, and T. S. Lane, The structure of bow shocks formed by the interaction of pulsed-power driven magnetised plasma flows with conducting obstacles, *Physics of Plasmas* **24**, 072713 (2017).
 - [23] I. H. Mitchell, J. M. Bayley, J. P. Chittenden, J. F. Worley, A. E. Dangor, M. G. Haines, and P. Choi, A high impedance mega-ampere generator for fiber z-pinch experiments, *Review of Scientific Instruments* **67**, 1533 (1996).
 - [24] S. V. Lebedev, L. Suttle, G. F. Swadling, M. Bennett, S. N. Bland, G. C. Burdiak, D. Burgess, J. P. Chittenden, A. Ciardi, A. Clemens, P. De Grouchy, G. N. Hall, J. D. Hare, N. Kalmoni, N. Niasse, S. Patankar, L. Sheng, R. A. Smith, F. Suzuki-Vidal, J. Yuan, A. Frank, E. G. Blackman, and R. P. Drake, The formation of reverse shocks in magnetized high energy density supersonic plasma flows, *Physics of Plasmas* **21**, 056305 (2014).
 - [25] J. P. Chittenden, S. V. Lebedev, B. V. Oliver, E. P. Yu, and M. E. Cuneo, Equilibrium flow structures and scaling of implosion trajectories in wire array Z pinches, *Physics of Plasmas* **11**, 1118 (2004).
 - [26] G. F. Swadling, S. V. Lebedev, G. N. Hall, S. Patankar, N. H. Stewart, R. A. Smith, A. J. Harvey-Thompson, G. C. Burdiak, P. De Grouchy, J. Skidmore, L. Suttle, F. Suzuki-Vidal, S. N. Bland, K. H. Kwek, L. Pickworth, M. Bennett, J. D. Hare, W. Rozmus, and J. Yuan, Diagnosing collisions of magnetized, high energy density plasma flows using a combination of collective Thomson scattering, Faraday rotation, and interferometry (invited), *Review of Scientific Instruments* **85**, 11E502 (2014).
 - [27] J. D. Hare, J. MacDonald, S. N. Bland, J. Dranczewski, J. W. D. Halliday, S. V. Lebedev, L. G. Suttle, E. R. Tubman, and W. Rozmus, Two-Colour Interferometry and Thomson Scattering Measurements of a Plasma Gun, *Plasma Physics and Controlled Fusion* **61**, 085012 (2019).
 - [28] D. R. Russell, *Bow Shock Interaction Experiments in a Magnetised Collisional Plasma*, Ph.D. thesis, Imperial College London (2021).
 - [29] L. G. Suttle, J. D. Hare, J. W. Halliday, S. Merlini, D. R. Russell, E. R. Tubman, V. Valenzuela-Villaseca, W. Rozmus, C. Bruulsema, and S. V. Lebedev, Collective optical Thomson scattering in pulsed-power driven high energy density physics experiments (invited), *Review of Scientific Instruments* **92**, 033542 (2021).
 - [30] D. H. Froula, S. H. Glenzer, N. C. Luhmann Jr., and J. Sheffield, *Plasma scattering of electromagnetic radiation: theory and measurement techniques*, 2nd ed. (Academic Press, New York, 2011).
 - [31] J. D. Hare, *High Energy Density Magnetic Reconnection Experiments in Colliding Carbon Plasma Flows*, Ph.D. thesis, Imperial College London (2017).
 - [32] N.-P. L. Niasse, *Development of a Pseudo Non-LTE model for Z-pinch simulations*, Ph.D. thesis, Imperial College London (2011).
 - [33] J. P. Edmiston and C. F. Kennel, A parametric survey of the first critical Mach number for a fast MHD shock, *Journal of Plasma Physics* **32**, 429 (1984).
 - [34] C. F. Kennel, J. P. Edmiston, and T. Hada, A Quarter Century of Collisionless Shock Research, in *Collisionless Shocks in the Heliosphere: A Tutorial Review* (American Geophysical Union (AGU), 1985).
 - [35] F. Suzuki-Vidal, S. V. Lebedev, A. Ciardi, L. A. Pickworth, R. Rodriguez, J. M. Gil, G. Espinosa, P. Hartigan, G. F. Swadling, J. Skidmore, G. N. Hall, M. Bennett, S. N. Bland, G. Burdiak, P. De Grouchy, J. Music, L. Suttle, E. Hansen, and A. Frank, Bow shock fragmentation driven by a thermal instability in laboratory astrophysics experiments, *The Astrophysical Journal* **815**, 96 (2015).
 - [36] A. J. Cunningham, A. Frank, P. Varnière, S. Mitran, and T. W. Jones, Simulating magnetohydrodynamical flow with constrained transport and adaptive mesh refinement: Algorithms and tests of the AstroBEAR code, *Astrophysical Journal, Supplement Series* **182**, 519 (2009).
 - [37] J. J. Carroll-Nellenback, B. Shroyer, A. Frank, and C. Ding, Efficient parallelization for AMR MHD multiphysics calculations; implementation in AstroBEAR, *Journal of Computational Physics* **236**, 461 (2013).